



A method for estimating lithium-ion battery state of health based on physics-informed hybrid neural network

Yufu Luo , Shaoxiao Ju, Peichao Li *, Hengyun Zhang

School of Mechanical and Automotive Engineering, Shanghai University of Engineering Science, Shanghai 201620, PR China



ARTICLE INFO

Keywords:
Lithium-ion battery
State of health
Aging mechanism
Physical information
Data-driven

ABSTRACT

Lithium-ion batteries (LIBs) are widely used in portable electronic devices and electric vehicles due to their high energy density and long cycle life. However, aging is inevitable during battery cycling, leading to capacity degradation and performance deterioration, which in turn affects the accuracy of state of health (SOH) estimation. To address these issues, this paper proposes a physics-information hybrid neural network (PIHNN). By integrating the electrochemical-thermal-mechanical-side reaction coupling (ETMS) aging model with data-driven methods, the proposed framework achieves accurate capacity loss prediction. The PIHNN framework innovatively introduces membrane resistance as a key health indicator. A physical constraint term, based on the monotonic relationship between membrane resistance and capacity loss, is embedded to enhance physical consistency and prediction accuracy. Additionally, Bayesian optimization algorithm (BOA) is employed for efficient hyperparameter tuning, further improving model performance and computational efficiency. The results demonstrate that under different operating conditions (1C, 0.5C, and 2C), the PIHNN significantly outperforms traditional models in terms of mean absolute error (MAE) and root mean square error (RMSE). The model exhibits superior predictive performance and robustness. In addition, validation on a publicly available dataset from Oxford University reduces MAE and RMSE to below 0.5 %.

1. Introduction

In recent years, the number of LIBs in use has been growing at an unprecedented rate. LIBs, with their high energy density, low self-discharge rate, and long lifespan, have become the primary energy storage solution for portable electronic devices, electric vehicles, and other applications [1–3]. While the rapid proliferation of LIBs has brought significant convenience, concerns about their aging and safety have garnered increasing attention [4,5]. Battery aging is inevitable during its service life, leading to capacity decline and resistance increase. To ensure the long-term, safe, and reliable operation of LIBs, appropriate maintenance and control, including SOH estimation, are essential. The SOH is defined as the ratio of the current available capacity to the initial capacity [6]. It reflects the degree of performance degradation during charge-discharge cycles and is a key parameter influencing battery reliability and safety. Accurate SOH estimation is particularly crucial for battery management systems (BMS) in electric vehicles equipped with LIBs.

Currently, SOH estimation methods for LIBs can be categorized into three main approaches: physical model-based, data-driven, and hybrid

methods. Physical models often rely on multiphysics coupling electrochemical frameworks to simulate battery mechanisms and evaluate aging performance and lifespan. For example, Yang et al. developed an electrochemical model incorporating side reactions of solid electrolyte interphase (SEI) lithium plating, capturing the transition from linear to nonlinear capacity degradation and predicting capacity loss [7]. Tang et al. combined electrochemical and thermal models to construct an electrochemical-thermal coupled degradation model, improving lifespan prediction accuracy [8]. Chen et al. developed an electrochemical-thermal-aging coupled model capable of simulating LIB performance and SOH, achieving an SOH prediction error below 0.5 % across multiple battery types [9]. Luo et al. introduced an electrochemical-thermal-mechanical coupled model that considers stress effects on capacity fade, providing deeper insights into the interplay of physical processes during battery aging [10]. These models, by comprehensively considering real electrochemical processes, enable a more accurate and reasonable SOH evaluation.

Due to the complex electrochemical characteristics and multiphysics coupling behavior of LIBs, traditional physics-based models face limitations in terms of real-time performance and adaptability. Therefore, real-time estimation of LIBs SOH is particularly important. It can

* Corresponding author.

E-mail address: wiselee18@163.com (P. Li).

Nomenclature

S_a	Specific area of the porous electrode (m^{-1})
α	Cathodic transfer coefficient
k	reaction rate ($\text{m}^{2.5} \text{ mol}^{-0.5} \text{ s}^{-1}$)
F	Faraday's constant (C mol^{-1})
T	Temperature (K)
η	Over potential (V)
R	Universal gas constant ($\text{J mol}^{-1} \text{ K}^{-1}$)
i_0	Exchange current density (A m^{-2})
c	Concentration (mol m^{-3})
ϕ_s	Solid phase potential (V)
ϕ_l	Electrolyte potential (V)
L_{neg}	Negative thickness (μm)
$E_{eq,i}$	Equilibrium potential (V)
E_a	Activation energy (kJ mol)
σ_h	Hydrostatic stress (GPa)
ρ_{SEI}	SEI density (kg m^{-3})
ρ_{Li}	Lithium density (kg m^{-3})
CNN-GRU-A	CNN-GRU-Attention
HF	Health feature
CCCT	Constant current charge time

overcome these limitations, promptly detect battery degradation trends, extend battery lifespan, enhance safety, and optimize energy management to ensure system performance and safety [11]. Data-driven methods have gained traction for SOH estimation due to their strong capability to model complex nonlinear relationships [12]. These methods improve estimation accuracy and efficiency and exhibit excellent adaptability and scalability in practical BMS. Zhu et al. leveraged aging mechanisms and used constant current charging time as a feature for SOH estimation with a linear regression model, achieving an error below 1.2 % [13]. Deng et al. proposed a capacity prediction method based on charging data using sequence-to-sequence (Seq2Seq) and Gaussian process regression (GPR), with prediction errors under 1.6 % [14]. Huang et al. employed transfer learning to achieve high-precision aging trajectory and remaining useful life (RUL) prediction using limited cycle data [15]. Gao et al. designed a multiscale RUL prediction framework based on variational mode decomposition (VMD) and ensemble machine learning, with an average error below 1.5 % [16]. Liu et al. used IC curve peak interval features and an LSTM-based model to reduce data requirements while maintaining prediction errors below 1.18 % [17]. Zheng et al. developed a residual convolution and transformer-based method (R-TNet) for SOH estimation with RMSE below 1.6 % [18]. Li et al. combined electrochemical impedance spectroscopy (EIS) and an improved equivalent circuit model (ECM), achieving an average RMSE of 1.77 % under varying temperatures [19]. Despite their efficiency, data-driven methods often lack physical interpretability and consistency due to their limited reliance on aging mechanisms, potentially leading to predictions that conflict with physical laws.

In recent years, the integration of physical information with data-driven methods has become an important research direction in the field of LIBs state estimation, aiming to overcome the limitations of purely data-driven approaches in terms of interpretability and physical consistency. Notably, the 2024 Nobel Prize in Physics was awarded to pioneers in the field of artificial intelligence, John Hopfield and Geoffrey Hinton, for their fundamental contributions to artificial neural networks and machine learning. Their work provides the theoretical foundation for combining physical models with data-driven methods, promoting the widespread application of artificial intelligence in scientific research. Currently, research on physics-informed neural networks (PINNs) can be broadly classified into three types. The first type is represented by the

classical PINN framework proposed by Raissi et al. in 2019 [20]. This method incorporates physical constraints from nonlinear partial differential equations into the loss function of neural networks and uses automatic differentiation to solve both forward and inverse problems. Due to its solid theoretical foundation, wide applicability, and strong versatility, it is considered a cornerstone in the field of PINNs. Dai et al. proposed an improved single-particle model (SPM) [21], which combines the PINN framework to account for the electrolyte dynamics in LIBs. By designing a loss function with physical constraints, they used neural networks to efficiently solve the lithium-ion concentration distribution in the electrolyte, significantly improving model accuracy under high-rate conditions. At the same time, the computational efficiency was improved by 20.8 %, and the maximum relative error was only 1.2 %. Wang et al. further proposed a PINN framework for parameter identification in LIBs electrochemical models (EM) [22], employing a "divide and conquer" strategy to categorize parameters into open-circuit voltage (OCV) related parameters, kinetic parameters, and electrolyte parameters, embedding physical laws into the neural network to optimize the loss function. This method performed excellently in model validation with known parameters, successfully identifying unknown parameters of actual batteries, and accurately simulating their dynamic characteristics. However, the application of this PINN framework in LIBs SOH estimation still faces challenges. The second type of PINN framework integrates multi-physics fields and data-driven methods to address complex state estimation problems. Li et al. developed a PINN framework combining physical models and deep learning [23] to estimate the internal state of LIBs electrode layers. They generated a large amount of simulation data using a high-fidelity electrochemical-thermal model to train a bidirectional long short-term memory (BiLSTM) network, enabling precise estimation of lithium-ion concentration and potential in the electrode and electrolyte, with a maximum error below 3 %. This method demonstrated good robustness and generalization ability under different environmental temperatures and sensor noise. Subsequently, Pang et al. proposed a PINN framework combining physical information and BiLSTM for estimating the heat generation rate (HGR) of LIBs [24]. By injecting physical variables from a single-particle model combined with thermodynamics (SPMT) into the BiLSTM network and using Bayesian optimization to tune network parameters, the method achieved average errors of 0.542 kW/m³ and 1.428 kW/m³ under dynamic stress tests (DST) and worldwide harmonized light vehicle test procedure (WLTP) conditions, respectively, showcasing strong predictive performance. Both works highlight the vast potential of combining physical information with data-driven methods in the application of PINNs for LIBs state estimation. The third type of PINN framework builds upon data-driven methods, further enhancing the model's physical consistency and interpretability by incorporating physical constraints into the loss function. Wang et al. proposed a PINN framework for SOH estimation of LIBs [25], which integrates empirical models of battery degradation with state-space equations. This method uses neural networks to capture complex battery degradation dynamics, while extracting universal features from short-term data before full battery charge to enhance model adaptability and generalization. Experiments demonstrated that the framework achieved an average absolute percentage error (MAPE) of <0.87 % across four large datasets, and performed excellently in small-sample learning and transfer learning tasks, but still faces challenges in noise and dynamic operating conditions.

Currently, the multiphysics coupling theories related to side reactions in batteries remain underdeveloped, and the description of battery aging processes is relatively limited. Therefore, constructing a multiphysics coupling model capable of comprehensively simulating the internal physical processes of batteries is crucial. However, traditional models face significant challenges in achieving real-time SOH estimation due to their high complexity. In contrast, data-driven methods have significantly improved the efficiency of SOH estimation [26–28], but lack physical interpretability and integration of physical features. To

overcome the limitations of physical models and data-driven models, many researchers have proposed hybrid models that combine physical information with data-driven approaches [29]. Currently, PINN models still exhibit significant limitations in capturing battery aging mechanisms. The continuous growth of the solid electrolyte interface (SEI) layer is the primary cause of calendar aging [30,31], directly leading to an increase in membrane resistance. However, most studies have not fully considered the impact of SEI layer growth mechanisms on LIBs aging.

To address the aforementioned issues, this paper develops a physics-based multiphysics coupling aging model for LIBs and proposes a PIHNN. Compared to the conventional PINNs in the literature, this study incorporates the impact of SEI layer growth on battery aging. Specifically, a hybrid feature set is utilized, including external features such as current and temperature during charge-discharge cycles. Additionally, a well-established and accurate ETMS model is employed to extract internal physical features related to aging, such as the thickness of the byproduct film from side reactions. This approach provides a detailed description of the capacity loss mechanism, with these multi-source features being continuously fed into the constructed network model. During the neural network training phase, physical knowledge embedded in the data is used as a constraint, and a physics-informed loss function is integrated into the training process to enhance the model's physical consistency, leading to the development of PIHNN. As the number of cycles increases, side reactions gradually consume cyclable lithium, shortening battery lifespan. This process is accompanied by SEI layer thickening, which results in a significant increase in membrane resistance. Overall, LIBs exhibit an increasing trend in membrane resistance during cyclic aging [10]. Given the strong monotonic relationship between membrane resistance and capacity loss, monitoring membrane resistance enables a more effective estimation of battery health. This approach not only improves the accuracy and robustness of SOH estimation but also provides new perspectives and tools for an in-depth understanding of battery aging behavior. The specific contributions are as follows:

- (1) A physics-based ETMS aging model for LIBs is developed. This model accounts for the effects of reactant concentration, temperature, current rate, and other physical parameters. By incorporating these factors, the proposed model achieves higher physical fidelity, and its accuracy and reliability are thoroughly validated.
- (2) Membrane resistance is introduced as a key feature variable for SOH estimation. The influence of membrane resistance on capacity loss is analyzed from both mechanistic and mathematical perspectives.
- (3) A PIHNN model is proposed, embedding the monotonic relationship between membrane resistance and capacity loss as a physical constraint into the network, thereby enhancing the model's physical interpretability and consistency.
- (4) The model's performance is validated under various operating conditions and on the publicly available dataset from Oxford University.

The remainder of this paper is organized as follows: Section 2 introduces the physical model, followed by the physics-informed data-driven model in Section 3. Section 4 presents experimental validation and analysis, while Section 5 concludes the study with a summary and outlook.

2. Physics-based cell modeling

2.1. Physical model

The electrochemical-thermal-mechanical (ETM) model used in this study is primarily based on our previous work [32]. Unlike traditional

aging models that do not fully rely on physics-based calculations for side reactions, this study computes side reactions by considering the underlying electrochemical and thermal physical processes. The model focuses on incorporating the effects of physical parameters such as reactant concentration, temperature, and charge-discharge current.

The exchange current density of the SEI side reaction can be expressed as

$$i_{0,SEI} = nFk_{SEI} \cdot \exp\left(\frac{E_{a,SEI}}{RT}\right) c_{EC}^{1-\alpha} c_{cycle}^{\alpha} \frac{S_{a,neg} L_{neg} i_{loc}}{i_{1C}} \quad (1)$$

where k_{SEI} is the initial reaction rate constant for SEI formation, α is the charge transfer coefficient, c_{EC} is the concentration of electrolyte solvent, c_{cycle} is the lithium-ion concentration during cycling, i_{loc} is the reaction local current density, i_{1C} is the reaction current at a 1C current rate.

Studies have shown that SEI formation is an irreversible reduction process [33]. Accordingly, the reaction kinetics equation for SEI formation is expressed as

$$i_{SEI,form} = -i_{0,SEI} \exp\left(-\frac{\alpha_{SEI} F}{RT} \eta_{SEI,form}\right) \quad (2)$$

The exchange current density for the lithium plating side reaction can be expressed as

$$i_{0,lpl} = nFk_{0,Li} \exp\left(\frac{E_{a,Li}}{RT}\right) (c_l)^{1-\alpha} (c_{cycle})^{\alpha} \left(\frac{S_{a,neg} L_{neg} i_{loc}}{i_{1C}}\right) \quad (3)$$

where $k_{0,Li}$ is the reaction rate constant of lithium plating, c_l is the lithium-ion concentration in the electrolyte.

Studies suggest that lithium plating is a reversible redox process [34]. Therefore, the reaction kinetics of lithium plating is described using the Butler-Volmer (B-V) equation.

$$i_{lpl} = i_{0,lpl} \left(\exp\left(\frac{\alpha_{lpl} F}{RT} \eta_{lpl}\right) \right), \eta_{lpl} \leq 0V \quad (4)$$

In addition, due to the involvement of side reactions, certain equations in the baseline ETM model need modifications to account for the effects of these processes. Consequently, the overpotential for the particle intercalation reaction is expressed as

$$\eta_i = \emptyset_s - \emptyset_l - E_{Eq,i} - \frac{\partial E_{Eq,i}}{\partial T} (T - T_{ref}) - \frac{\Omega \sigma_h}{F} - i_{loc,i} R_{film} \quad (5)$$

where, $i_{loc,i}$ represents the local current density of the main reaction, and R_{film} is the resistance of the side reaction product film to lithium-ion transport. This resistance can be described in terms of the film thickness and the film conductivity:

$$R_{film} = \frac{\delta_{film,p}}{\sigma_{film}} \quad (6)$$

Furthermore, side reactions will lead to the growth of the composite film on the particle surface, composed of SEI and metallic lithium. This growth follows Faraday's law of deposition, expressed as

$$\delta_{film,p} = \delta_{0,film} + \frac{1}{S_{a,n}} \left(\frac{c_{SEI} M_{SEI}}{\rho_{SEI}} + \frac{c_{Li,lpl} M_{Li}}{\rho_{Li}} \right) \quad (7)$$

where, $\delta_{0,film}$ represents the initial film thickness, and $S_{a,n}$ is the specific surface area of the negative electrode. The concentrations of SEI reaction products c_{SEI} and lithium plating products $c_{Li,lpl}$ are expressed based on Faraday's law as

$$\frac{dc_{SEI}}{dt} = -\frac{S_{a,n} i_{SEI,form}}{F} \quad (8)$$

$$\frac{dc_{Li,lpl}}{dt} = -\frac{S_{a,n} i_{lpl}}{F} \quad (9)$$

In summary, this study establishes a physics-based side reaction model that considers both SEI formation and lithium plating side reactions, thereby enhancing the accuracy of long-cycle life predictions for battery aging. The kinetic equations for side reactions in the model are derived based on the underlying physical processes, incorporating the effects of potential, concentration, current rate, and temperature variations. On one hand, the physics-based model effectively simulates battery aging under varying temperatures and current rates. On the other hand, it facilitates in-depth mechanistic analysis, laying the groundwork for identifying more physical parameters that accurately describe aging behavior in future research.

2.2. Numerical solution and data acquisition

A commercial finite element analysis software, COMSOL Multiphysics 6.2, is used to establish the physical model and conduct numerical simulations (the validation of the physical model is provided in [Section 4.1](#)). To train and test the PIHNN method for battery SOH estimation introduced in [Section 3](#), capacity loss data are collected under three different operating conditions: ambient temperature of 25 °C with charge-discharge rates of 1C, 0.5C, and 2C. In the capacity loss calculation, additional considerations are made regarding the impact of lithium plating, extending the applicability of the improved model. The capacity degradation and SOH of LIBs are predicted by calculating the loss of cyclable lithium. The collected data are shown in [Fig. 1](#), which presents the aging curve of the tested battery under 1C charge-discharge

conditions. As the cycle number increases, the discharge termination time shifts significantly earlier. Given that the discharge current remains constant at -2 A, this indicates a gradual reduction in discharge capacity. During the charging phase, the loss of cyclable lithium ions causes the end time of constant-current charging to move earlier, while the duration of constant-voltage charging increases. This trend suggests an intensification of side reactions. [Fig. 1. b](#) presents the surface temperature variation of the tested battery under 1C charge-discharge conditions. As the cycle number increases, the peak surface temperature in each cycle gradually rises. From a mechanistic perspective, in addition to the primary reaction of lithium-ion intercalation and deintercalation, electrochemical side reactions also occur, leading to increased heat generation and further temperature rise.

The initial capacity of the battery is defined as [10]

$$C_0 = F \varepsilon_n L_n A_{cell} c_{s,max,n} \quad (10)$$

where L_n is the anode length, A_{cell} is the anode cross-sectional area, and $c_{s,max,n}$ is the maximum lithium concentration in the anode.

Similarly, the relationship between capacity loss and the concentration of side reaction products can be defined as

$$C_{loss} = F \varepsilon_s n L_n A_{cell} (c_{Li,pl} + c_{SEI}) \quad (11)$$

The State of Health (SOH) of the battery is defined as the ratio of the current available capacity to the initial capacity [6]:

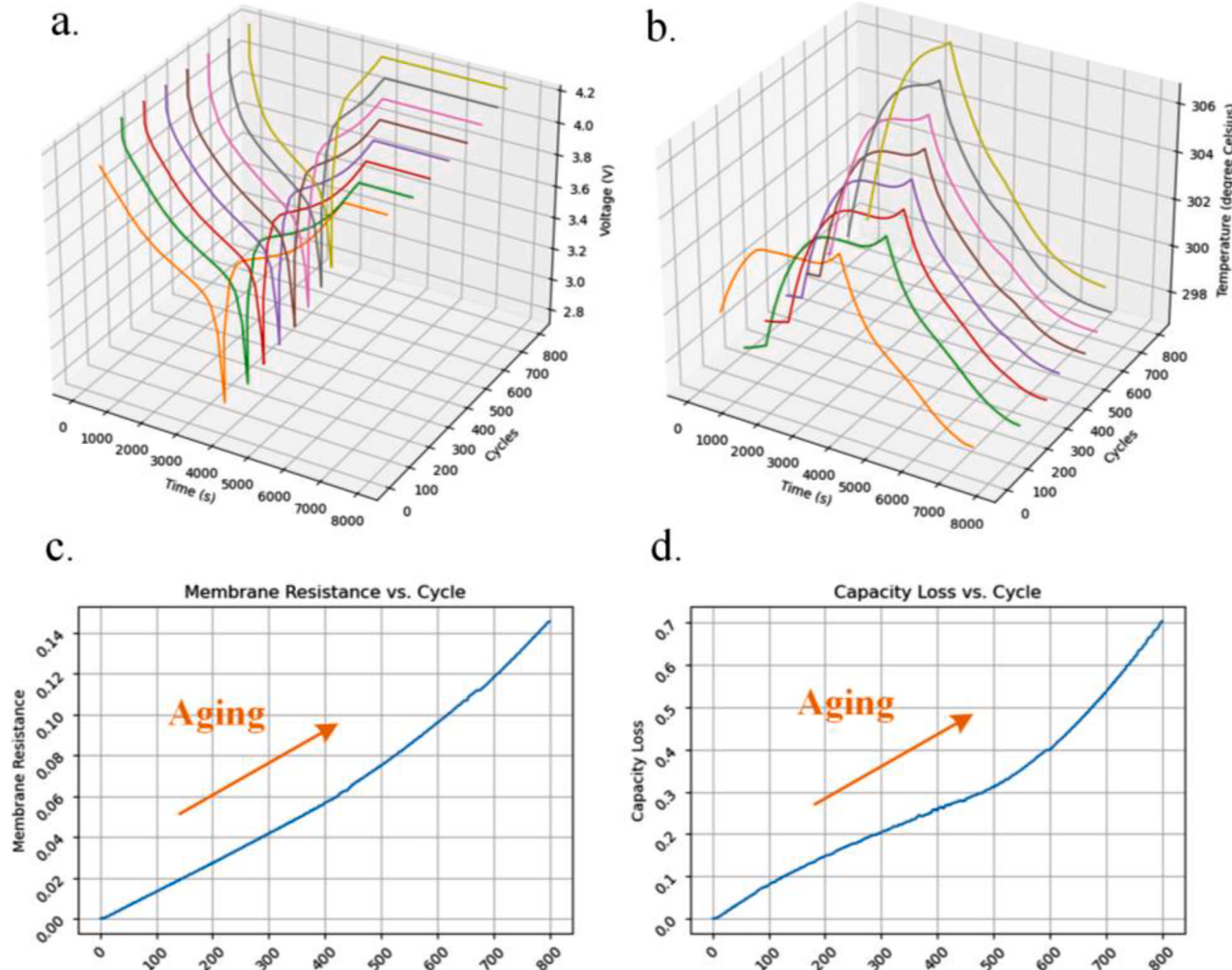


Fig. 1. Battery aging curve.

$$\text{SOH} = \frac{C_0 - G_{\text{loss}}}{C_0} \quad (12)$$

Eq. (12) represents the SOH calculation model used in this study. From the model, it is evident that the SOH calculation is directly proportional to the concentration of side reaction products. Therefore, this study estimates capacity loss and equates it to SOH for analysis.

3. PINN framework for SOH estimation

3.1. Data preprocessing

Considering that data normalization is a prerequisite for constructing and training the hybrid neural network, Min-Max normalization is applied to eliminate the scale differences among various indicators and ensure comparability between them. Each feature sequence is normalized to the range [0,1] using the following equation:

$$X_{\text{norm}} = \frac{X - X_{\min}}{X_{\max} - X_{\min}} \quad (13)$$

where, X_{norm} is the normalized value, X is the original data value, X_{\min} is the minimum value of the feature data, and X_{\max} is the maximum value of the feature data.

3.2. Feature extraction

To construct the PIHNN model capable of accurately predicting battery capacity loss, it is essential to extract feature variables closely related to capacity loss from extensive datasets. This study initially selected commonly used feature variables reported in the literature [35–37], such as the maximum surface temperature of the battery and the constant-current charging time. The relationships between these variables and capacity loss were verified through correlation analysis. On this basis, the study innovatively introduced health factors with stronger physical significance as feature variables. These health factors were further investigated for their potential advantages in capacity loss prediction through mechanistic and correlation analyses.

This study proposes membrane resistance as a feature variable. To scientifically validate the relationship between feature variables and capacity loss, Spearman correlation analysis was employed. Spearman correlation is a non-parametric statistical method used to measure the monotonic relationship between two variables. The formula for calculating the correlation coefficient ρ is as follows:

$$\rho = 1 - \frac{6 \sum d_i^2}{n(n^2 - 1)} \quad (14)$$

where, d_i is the difference between the ranks of the two variables, and n is the sample size.

Table 1 presents the Spearman correlation analysis results between capacity loss and constant-current charging time, temperature, and membrane resistance. The analysis indicates a strong negative correlation between constant-current charging time and capacity loss, with a correlation coefficient of -0.999974 . This suggests that as the constant-current charging time increases, capacity loss tends to decrease. Temperature shows a strong positive correlation with capacity loss, with a correlation coefficient of 0.999929 , indicating that high-temperature environments accelerate capacity degradation. Similarly, membrane

Table 1
Spearman correlation coefficient analysis related to capacity loss.

HF	Value
CCCT	-0.999974
T	0.999929
R_{film}	0.999978

resistance exhibits a strong positive correlation with capacity loss, with a correlation coefficient of 0.999978 . This result validates the significance of membrane resistance as a health factor and its substantial physical relevance. These findings demonstrate that membrane resistance holds high reference value for predicting capacity loss and can serve as a critical input feature for the PIHNN model.

Further analysis reveals a monotonic increasing relationship between membrane resistance and capacity loss, as shown in Fig. 2. The increase in membrane resistance indicates a gradual growth in the thickness of the SEI layer, reflecting an extended lithium-ion transport path and enhanced charge transfer resistance within the film. This physical process restricts the availability of active lithium, thereby accelerating capacity degradation. Fig. 2 visually illustrates the intrinsic correlation between membrane resistance and capacity loss through a data trend line, further validating the physical significance and predictive value of membrane resistance as a key health factor influencing battery capacity.

Based on the above discussion, this study further explores the relationship between capacity loss and membrane resistance from a mechanistic perspective. The formation and thickening of the SEI layer are the primary causes of changes in membrane resistance. During SEI growth, a portion of lithium ions is consumed to form the new SEI layer, as shown in Eq. (7), reducing the number of active lithium ions available for cycling, which leads to capacity loss.

With increasing cycle numbers, the thickness of the SEI layer grows continuously, resulting in a significant increase in membrane resistance, as shown in Eq. (6). This increase in thickness further impacts membrane resistance and ultimately degrades the electrochemical performance of the battery, such as reducing charge/discharge efficiency, as shown in Eq. (5).

The aforementioned equations theoretically reveal the interrelationship between capacity loss and membrane resistance. An increase in membrane resistance not only hinders lithium-ion transport but also exacerbates electrode polarization. This effect is particularly pronounced under high-temperature conditions, where accelerated side reactions significantly enhance the SEI growth rate, increasing membrane resistance and ultimately impacting the cycle life and performance of the battery.

The primary reason for selecting membrane resistance as a feature variable lies in its ability to directly reflect the extent of irreversible side reactions within the battery and indirectly indicate changes in SEI thickness. Membrane resistance possesses clear physical significance, shows a strong correlation with capacity loss, and is driven by multiple factors in electrochemical processes (e.g., temperature, cycle count, and current density), making it a comprehensive indicator of battery capacity degradation. Moreover, membrane resistance is relatively easy to obtain in practical tests.

Thus, membrane resistance is chosen as a critical input feature for

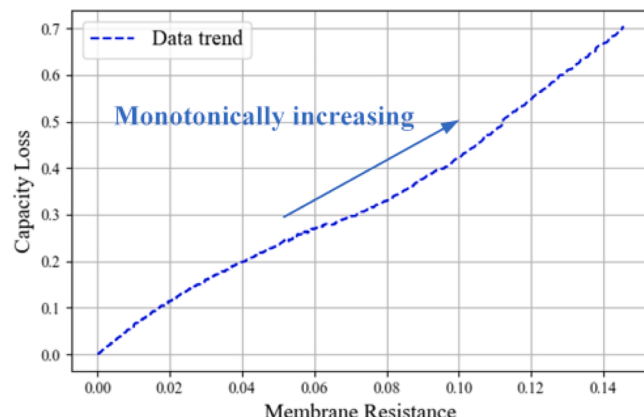


Fig. 2. Relationship curve between membrane resistance and capacity loss.

the PIHNN model to improve the accuracy of capacity loss predictions and enhance the model's physical interpretability.

3.3. CNN-GRU-Attention

The CNN module is designed to extract local features from the input data, specifically capturing short-term dependencies or local trends in time-series data. Through convolutional operations, CNN effectively identifies short-term variation patterns in battery feature variables, while offering advantages such as noise reduction and efficient feature extraction [38]. This module also reduces data dimensionality while retaining critical information, providing a concise and effective feature representation for subsequent modules.

The GRU module addresses long-term dependencies in time-series data, capturing the dynamic evolution of battery feature variables. Compared to traditional RNN models, the GRU structure introduces update and reset gates, which enhance the control of information flow and retention. This design mitigates the vanishing gradient problem while reducing computational complexity [39]. The GRU module models input sequence features along the temporal dimension, further improving the ability to predict capacity degradation. The four key expressions are as follows:

$$r_t = \sigma(W_r \cdot [h_{t-1}, x_t] + b_r) \quad (15)$$

$$z_t = \sigma(W_z \cdot [h_{t-1}, x_t] + b_z) \quad (16)$$

$$\bar{h}_t = \tanh(W_h \cdot [r_t * h_{t-1}, x_t] + b_h) \quad (17)$$

$$h_t = z_t * h_{t-1} + (1 - z_t) * \bar{h}_t \quad (18)$$

where, r_t represents the current reset gate signal, x_t denotes the input at the current time step, z_t is the current update gate signal, \bar{h}_t retains part of the current input and the previous output, and h_t represents the current output. W_r , W_z , W_h are weight matrices, while σ and \tanh are activation functions.

The Attention module assigns weighted importance to time-series features extracted by the GRU, emphasizing the most relevant features for capacity degradation prediction. By allocating different weights, the Attention mechanism dynamically focuses on critical moments of feature variation, enhancing both interpretability and prediction accuracy [40]. This module optimizes feature utilization by integrating contextual information, improving the model's ability to learn complex feature relationships.

By combining CNN, GRU, and Attention modules, this architecture efficiently extracts both local and global features while highlighting key characteristics, offering a comprehensive feature representation and

precise prediction capability for battery capacity degradation. Fig. 3 illustrates the structure of the CNN-GRU-Attention model.

3.4. BOA-based neural network

Reports suggest that the selection of hyperparameters significantly impacts the performance of network models, including computational cost and prediction accuracy [41]. Typically, hyperparameters in RNNs and their variants are determined using trial-and-error methods, relying heavily on empirical rules. This approach increases training time and complexity. Similar to other network architectures, the capacity loss prediction model proposed in this study requires careful consideration of hyperparameter optimization.

Compared to traditional grid search algorithms, the BOA efficiently tracks all historical evaluations, avoiding redundant computations for suboptimal hyperparameters and significantly improving optimization efficiency. Unlike population-based algorithms such as Particle Swarm Optimization, BOA requires no additional parameter settings, making it particularly suitable for optimizing objective functions with high computational costs. Literature shows that BOA can converge to an optimal solution with fewer iterations, making it widely applicable for hyperparameter optimization tasks [42].

Leveraging these advantages, this study introduces BOA to replace the traditional trial-and-error approach for optimizing the hyperparameters of the PIHNN-based model for capacity loss prediction. BOA's efficient search mechanism significantly reduces the computational cost of hyperparameter optimization while enhancing the model's predictive performance. The optimized hyperparameters under various operating conditions in this study are shown in Table 2.

3.5. Physically constrained neural network

To enhance the interpretability of the capacity loss prediction model, this study incorporates physical constraints to guide the training of the neural network. These constraints are based on the understanding of

Table 2
The hyperparameters of the neural network.

Operating Condition	1C	0.5C	2C
Conv filters	64	192	192
GRU units 1	192	64	256
GRU units 2	128	128	128
Dropout rate	0.2	0.2	0.4
Dense units	16	48	64
Learning rate	0.001	0.0003	0.0002

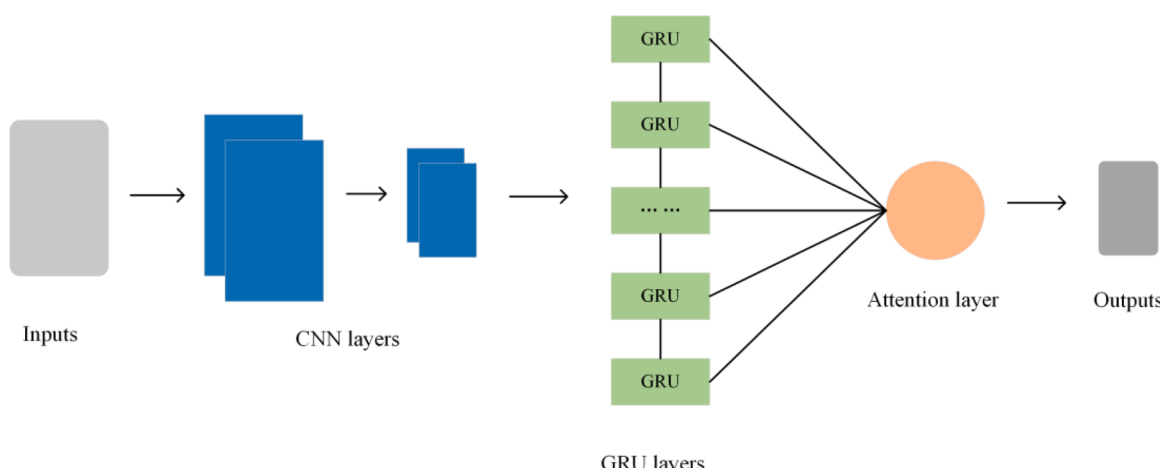


Fig. 3. CNN-GRU-Attention.

battery degradation mechanisms described in [Section 3.2](#) and effectively improve the model's accuracy and interpretability. As discussed in [Section 3.2](#), a monotonic relationship exists between capacity loss and membrane resistance. This physical information is translated into constraint conditions and integrated into the loss function of the neural network.

During model training, these constraints guide the model to adhere to the physical laws governing battery degradation, improving both its reliability and its ability to explain the mechanisms underlying capacity loss. This approach enables the model to achieve not only accurate predictions of capacity loss but also higher physical significance and credibility.

Traditional neural networks typically use Mean Squared Error (MSE) as the loss function to measure the difference between predicted and actual values. The MSE expression is as follows:

$$L_{Data} = MSE = \frac{1}{N} \sum_{t=1}^N (C_t^{true} - C_t^{pred})^2 \quad (19)$$

To further enhance the physical interpretability of the model, this study introduces a physical constraint term and integrates it into the loss function. This constraint is based on the monotonic relationship between membrane resistance and capacity loss. The constraint expression is as follows:

$$L_{physics} = \sum_{t=1}^{N-1} \text{ReLU}(-\Delta R_t \cdot \Delta C_t^{pred}) \quad (20)$$

In the expression, the ReLU function ($\text{ReLU}(x) = \max(0, x)$) is used to penalize cases that violate the physical constraint, ensuring the model adheres to the monotonic relationship where capacity loss increases with membrane resistance. Since $\Delta R_t > 0$, the equation can be simplified as

$$L_{physics} = \sum_{t=1}^{N-1} \text{ReLU}(-\Delta C_t^{pred}) \quad (21)$$

[Eq. \(21\)](#) is embedded into the loss function as a physical constraint.

The final loss function is composed of the data error term and the physical constraint term. Its expression is given as

$$L_{Total} = L_{Data} + \alpha L_{physics} \quad (22)$$

where, α is the weighting coefficient used to balance the impact of the data error term and the physical constraint term. This improved loss function not only effectively reduces prediction errors but also guides the model to adhere to the physical laws governing battery capacity degradation during training. This approach significantly enhances the reliability and interpretability of the model. To further enhance model interpretability, the integration of physical constraints not only improves prediction accuracy but also provides a clear theoretical foundation. During training, well-established electrochemical principles, such as the monotonic relationship between membrane resistance and capacity loss, are embedded to ensure that PIHNN's outputs are both mathematically optimal and physically meaningful. The interpretability of the model stems from its strict adherence to known physical laws governing LIBs, ensuring that each prediction aligns with fundamental physical principles. This design makes the reasoning behind model decisions more transparent and directly linked to underlying physical mechanisms, thereby enhancing the reliability and credibility of the results.

3.6. The PINN-based research framework

This paper proposes a PIHNN framework, as shown in [Fig. 4](#), for accurately estimating the SOH of LIBs under various operating conditions. First, a multiphysics coupling aging model is constructed and validated, enabling an in-depth analysis of capacity degradation mechanisms and the extraction of highly relevant feature variables. Among these, membrane resistance, as an innovative health factor, demonstrated significant physical significance.

Subsequently, a hybrid model integrating CNN, GRU, and Attention mechanisms was designed to capture the local and global dynamic features of capacity degradation. Additionally, BOA was introduced to efficiently configure and optimize hyperparameters. Finally, a physical

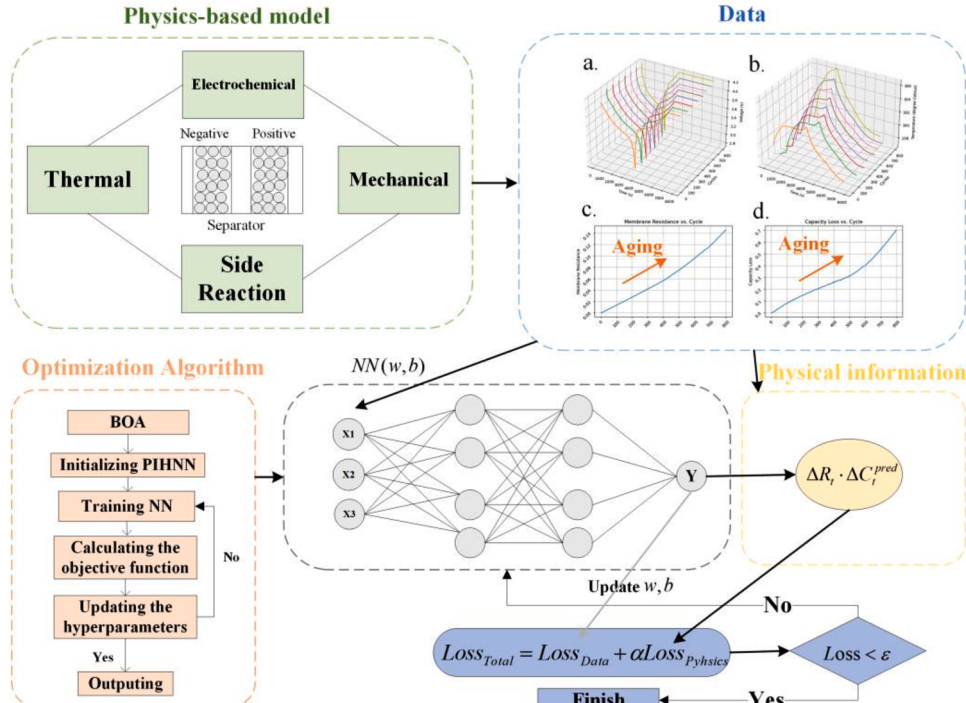


Fig. 4. Research framework.

constraint based on the monotonic relationship between membrane resistance and capacity loss was embedded into the model's loss function, enhancing its physical consistency and predictive reliability.

This framework demonstrated excellent performance in terms of accuracy, robustness, and physical interpretability, offering a novel approach and theoretical support for LIBs SOH estimation.

4. Results and discussion

In this study, the dataset was divided into a training set and a testing set, with 80 % of the data used for model training and the remaining 20 % for testing and validation. The results presented below are based on this data splitting strategy, demonstrating the effectiveness and accuracy of the proposed method by evaluating the performance of different models on the capacity loss prediction task. The performance of capacity loss estimation was validated using two key evaluation metrics: Mean Absolute Error (MAE) and Root Mean Squared Error (RMSE). Their formulas are as follows:

$$MAE = \frac{1}{n} \sum_{i=1}^n |Y_i - \hat{Y}_i| \quad (23)$$

$$RMSE = \sqrt{\frac{1}{n} \sum_{i=1}^n (Y_i - \hat{Y}_i)^2} \quad (24)$$

where, Y_i represents the true value of the i -th sample, \hat{Y}_i represents the predicted value of the i -th sample, n is the total number of samples, and i is the index of the sample.

4.1. Experimental validation of physics-based modeling

The LIBs used to validate the multiphysics coupling aging model in this study is the Sanyo UR18650E, which has a graphite anode and an NCM111 cathode (Li_y (Ni_{0.33}Co_{0.33}Mn_{0.33}) O₂). To verify the

proposed model, the computational results were compared with experimental data from Keil and Jossen [43]. In their study, the Sanyo battery, with a nominal capacity of 2.05 Ah, was tested. The coupled model was solved using COMSOL software. Boundary conditions were defined according to experimental setups, where the left side of the negative current collector was fixed, the right side of the positive current collector was subjected to an external normal load, and all other boundaries were assumed free. The experiments were conducted at 25 °C under various discharge rates (0.2C, 0.5C, 1C, and 2C) to measure discharge voltage and surface temperature during the first cycle. As shown in Fig. 5.a and b, the simulated voltage and temperature curves align well with experimental data, with RMSEs below 1 % for voltage and 3 % for temperature, confirming the model's strong performance at the battery's initial state.

The capacity degradation model was further validated using charge-discharge cycling tests. In the aging experiments, the temperature was maintained at 25 °C, and each cycle consisted of constant-current discharge at -2A to a cutoff voltage of 2.75 V, constant-current charge at 2A to a cutoff voltage of 4.2 V, followed by constant-voltage charging at 0.1A with a 10 s rest period before the next cycle. Fig. 5.c compares the simulated capacity loss results with experimental data, showing good agreement between them. The RMSE of the simulated results is <4 %, verifying the accuracy of the model.

Additionally, the improved physics-based side reaction model demonstrated better agreement with experimental data compared to the unmodified model. The RMSE of the improved model was 3.62 %, while that of the unmodified model was 6.26 %. These results indicate that the proposed physics-based electrochemical-thermal-mechanical side reaction coupled model is more reasonable and accurately captures the battery degradation mechanisms.

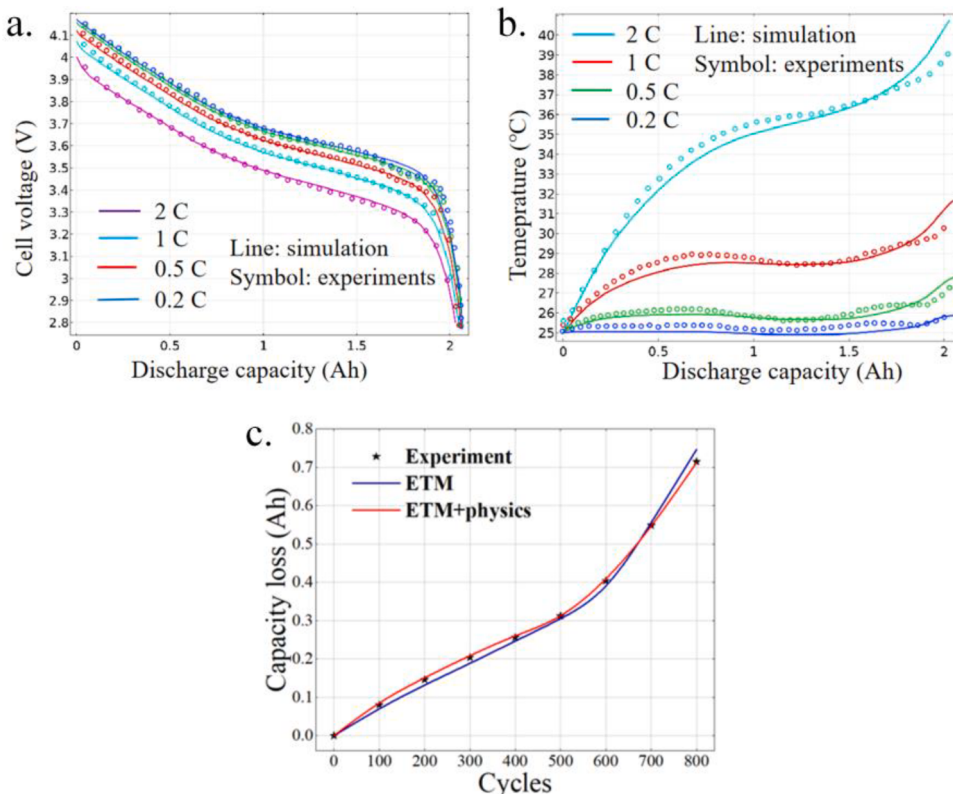


Fig. 5. Comparison of experimental and simulation data.

4.2. Validation under different operating conditions with and without Bayesian optimization

To verify the effectiveness of the BOA in the hybrid neural network, a comparative analysis was conducted under different operating conditions (e.g., 1C, 0.5C, and 2C). The performance differences between models with and without BOA-based hyperparameter optimization were evaluated. Fig. 6 visually illustrates these differences across various conditions.

The results demonstrate that the BOA-optimized model significantly outperformed the non-optimized model under all operating conditions. BOA effectively improved the model's capacity degradation prediction by rapidly converging to the optimal hyperparameter configuration. Additionally, BOA substantially reduced computational costs and errors, providing reliable support for the model's application in complex operating scenarios.

4.3. Validation under different operating conditions with and without membrane resistance

To validate the importance of membrane resistance (MR) as a feature in the hybrid model, comparative experiments were conducted under 1C, 0.5C, and 2C operating conditions. The results are presented in both tabular and graphical formats. As shown in Fig. 1, the fitting results demonstrate that the hybrid model incorporating MR aligns significantly better with actual capacity loss compared to the CNN-GRU-A model without MR, highlighting the notable improvement in prediction performance achieved by including the MR feature.

Additionally, as shown in Table 3, under 1C conditions, the hybrid model with MR achieved an MAE of 0.47 % and an RMSE of 0.54 %, compared to 0.61 % and 0.79 %, respectively, for the CNN-GRU-A model. Under 0.5C conditions, the hybrid model with MR yielded an MAE of 0.16 % and an RMSE of 0.54 %, outperforming the CNN-GRU-A model's values of 0.23 % and 0.33 %. Under 2C conditions, the hybrid model with MR achieved an MAE of 0.34 % and an RMSE of 0.41 %, again superior to the CNN-GRU-A model's 0.36 % and 0.42 %.

These results indicate that incorporating the MR feature significantly enhances the model's prediction accuracy under various operating conditions, while also improving its physical consistency. This provides critical support for the precise estimation of LIBs capacity degradation.

4.4. Validation under different operating conditions with and without physical constraint

This section explores the impact of physical information constraints on improving capacity loss prediction performance. By comparing the performance of different models under various operating conditions, the advantages of the proposed PIHNN in terms of accuracy and physical consistency are validated. Four models were evaluated for capacity loss prediction: the proposed PIHNN, CNN-GRU-A, CNN-GRU, and GRU. All models utilized BO for hyperparameter optimization and included MR as

Table 3

Comparison of models with and without MR under different operating conditions.

Operating condition	1C	0.5C	2C
MAE (%)	With MR	0.47	0.16
	CNN-GRU-A	0.61	0.36
RMSE (%)	With MR	0.54	0.22
	CNN-GRU-A	0.79	0.41

a feature variable. Only the PIHNN model incorporated physical information constraints into its loss function. Fig. 7 compares the performance of different models under various conditions, Fig. 8 highlights the error differences, and Table 4 provides detailed error metrics for each model.

Under standard conditions (1C), the PIHNN model achieved the best prediction accuracy, with MAE and RMSE of 0.29 % and 0.34 %, respectively, significantly outperforming other models. The CNN-GRU-A model, with MAE and RMSE of 0.47 % and 0.54 %, captured capacity loss trends well but lagged behind PIHNN in accuracy. The CNN-GRU and GRU models exhibited MAE and RMSE of 1.6 % and 1.8 %, and 1.8 % and 2.4 %, respectively, with lower global prediction accuracy and more substantial local deviations, particularly in stable conditions, reflecting their limited adaptability. Under low-rate conditions (0.5C), the PIHNN model maintained superior prediction performance, with MAE and RMSE of 0.15 % and 0.20 %, respectively, demonstrating robustness under stringent conditions. The CNN-GRU-A model, with MAE and RMSE of 0.16 % and 0.23 %, showed a slight decrease in predictive ability. The CNN-GRU and GRU models performed significantly worse, with MAE and RMSE of 0.25 % and 0.33 %, and 0.48 % and 0.71 %, respectively, indicating challenges in handling the complex variations at low discharge rates. Under high-rate conditions (2C), the PIHNN model again outperformed others, with MAE and RMSE of 0.19 % and 0.24 %, respectively. While the CNN-GRU-A model achieved MAE and RMSE of 0.34 % and 0.42 %, capturing trends reasonably well, its errors were larger compared to PIHNN. The CNN-GRU and GRU models had MAE and RMSE of 0.36 % and 0.45 %, and 0.30 % and 0.36 %, respectively, with relatively poor performance under the complex high-rate conditions, highlighting their limitations.

The PIHNN model consistently outperformed all other models across all conditions, particularly under low-rate and high-rate scenarios, showing better robustness and adaptability. By incorporating physical loss terms, the PIHNN model more accurately modeled capacity loss trends, improving the physical consistency of predictions. Compared to other models, PIHNN reduced MAE and RMSE by 25 %–40 % and 20 %–33 %, respectively, demonstrating its significant advantages. The CNN-GRU-A model was the second-best performer, effectively capturing some features via the Attention mechanism. However, its lack of physical constraints limited its generalization capability under complex conditions.

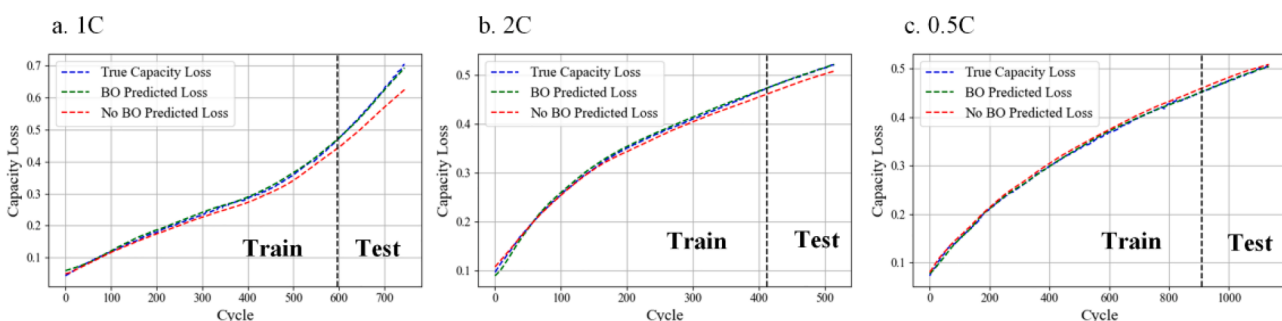


Fig. 6. Comparison of models with and without BOA under different operating conditions.

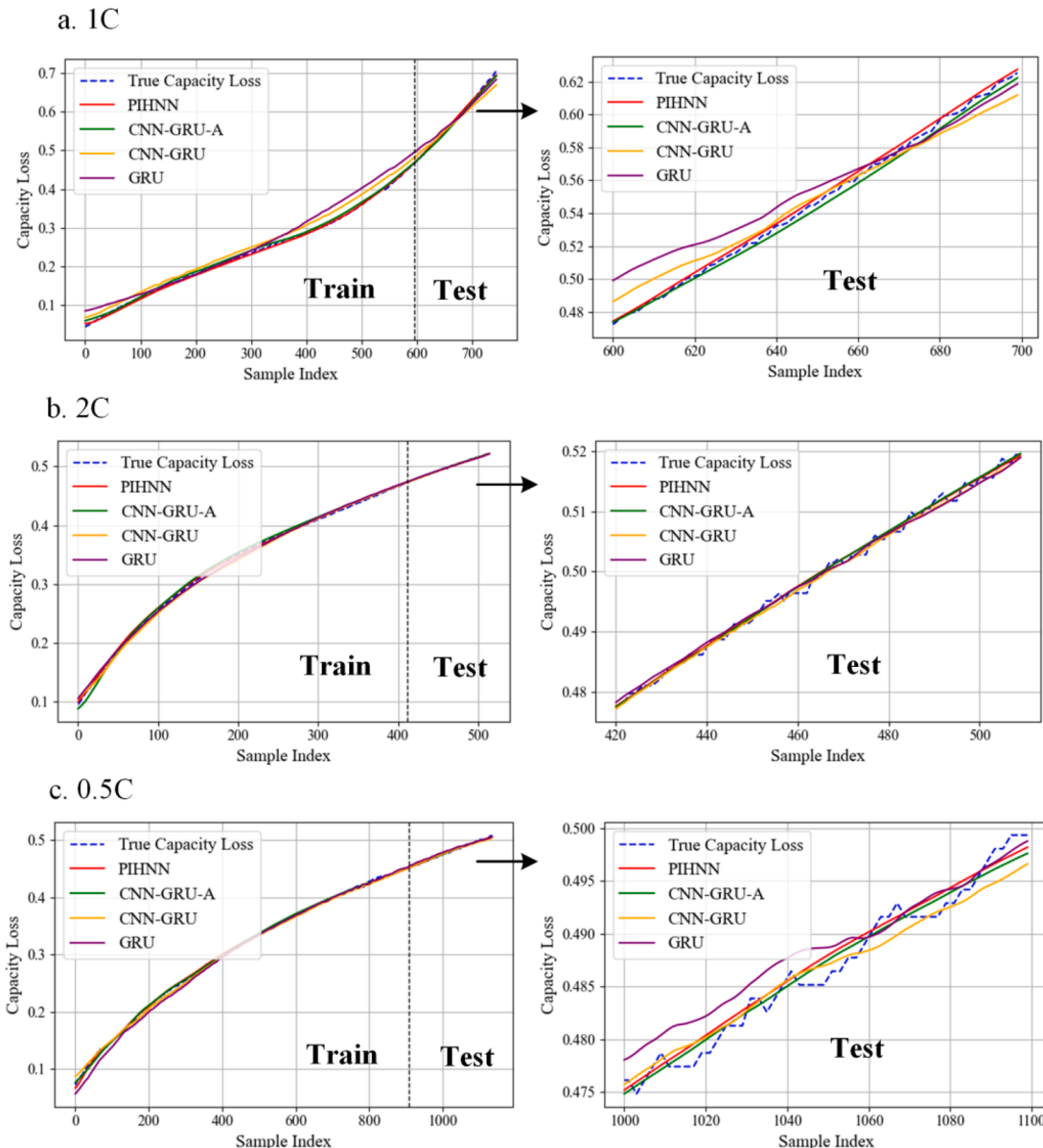


Fig. 7. Performance comparison of different models under various operating conditions.

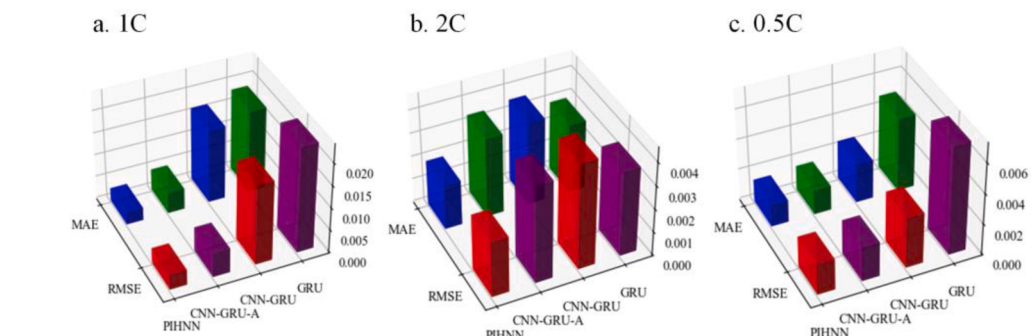


Fig. 8. Comparison of errors across different models under various operating conditions.

4.5. Validation on the Oxford University public dataset

To further validate the generality and effectiveness of the proposed PIHNN method, it was applied to the publicly available Oxford Battery

Dataset [44,45]. In the Oxford study, systematic cycling tests were conducted on eight Kokam pouch LIBs, labeled as Cell 1 to Cell 8. These batteries have a nominal capacity of 740 mAh and use a composite cathode material of lithium nickel cobalt oxide and lithium cobalt oxide,

Table 4

Comparison of errors across different models under various operating conditions.

Operating condition		1C	0.5C	2C
MAE (%)	PIHNN	0.29	0.15	0.19
	CNN-GRU-A	0.47	0.16	0.34
	CNN-GRU	1.6	0.25	0.36
	GRU	1.8	0.48	0.30
RMSE (%)	PIHNN	0.34	0.20	0.24
	CNN-GRU-A	0.54	0.23	0.42
	CNN-GRU	1.8	0.33	0.45
	GRU	2.4	0.71	0.36

paired with a graphite anode, representing a typical configuration in current LIBs technology. To simulate real-world usage scenarios for electric vehicles, the researchers designed a dynamic charge-discharge protocol. Specifically, the batteries underwent cycling at a 2C rate, with a standardized charging process conducted every 100 cycles: constant-current charging at 1C to 4.2 V, followed by a constant-voltage mode until the charging current dropped to a preset cutoff value. During the tests, key parameters such as time (t), voltage (V), temperature (T), and current (I) were recorded in real time to assess battery performance degradation.

The validation is performed on four randomly selected cells: 1, 3, 7, and 8. The results, shown in Fig. 9 and Table 5, demonstrate the performance of the PIHNN model on the Oxford dataset, further verifying its robustness and applicability.

4.6. Validation on the MIT public dataset

To further validate the generalization capability of the PIHNN method, we conducted comparative experiments on the MIT battery dataset, which includes 124 commercial LIBs that failed under fast-charging conditions [46]. These lithium iron phosphate (LFP)/graphite batteries, manufactured by A123 Systems (APR18650M1A), were cycled in horizontal cylindrical fixtures on a 30-channel Arbin LBT within a forced convection temperature chamber set at 48 °C. During the

Table 5

Comparison of prediction performance for different models on the Oxford battery dataset.

Cell		Cell 1	Cell 3	Cell 7	Cell 8
MAE (%)	PIHNN	0.19	0.37	0.44	0.38
	CNN-GRU-A	0.50	0.48	0.47	0.39
	CNN-GRU	0.45	0.73	0.44	0.39
	GRU	0.51	0.37	0.51	0.56
RMSE (%)	PIHNN	0.17	0.20	0.36	0.24
	CNN-GRU-A	0.46	0.33	0.38	0.33
	CNN-GRU	0.43	0.43	0.36	0.33
	GRU	0.47	0.21	0.48	0.53

charging phase, 72 different charging modes were formed by combining constant current fast-charging at various rates.

Based on two specific batteries (b3c18 and b3c34) from the MIT public dataset, the proposed PIHNN was compared with the PGTL-LSTM (physics-guided TL-LSTM) model presented in Reference [47]. Fig. 10 shows the prediction fitting curves obtained by PIHNN, demonstrating a strong alignment between the predicted and actual values. Table 6 further details the prediction errors of both models. Specifically, compared with PGTL-LSTM, PIHNN achieved reductions of 19.35 % and 8.33 % in terms of MAE for batteries b3c18 and b3c34, respectively. Regarding RMSE, PIHNN reduced the prediction error by 26.67 % for battery b3c18, while exhibiting a slight increase of 22.22 % for battery b3c34. Overall, the results indicate that PIHNN outperforms PGTL-LSTM, highlighting its excellent generalization capability.

5. Conclusions

This paper proposes a PIHNN for accurate SOH estimation of LIBs under various operating conditions. By constructing a multiphysics coupling model, the key mechanisms of capacity degradation were thoroughly analyzed, and membrane resistance was introduced for the first time as a critical health factor for SOH estimation. A hybrid framework combining CNN, GRU, and Attention mechanisms was designed, embedding a physical constraint term based on the monotonic

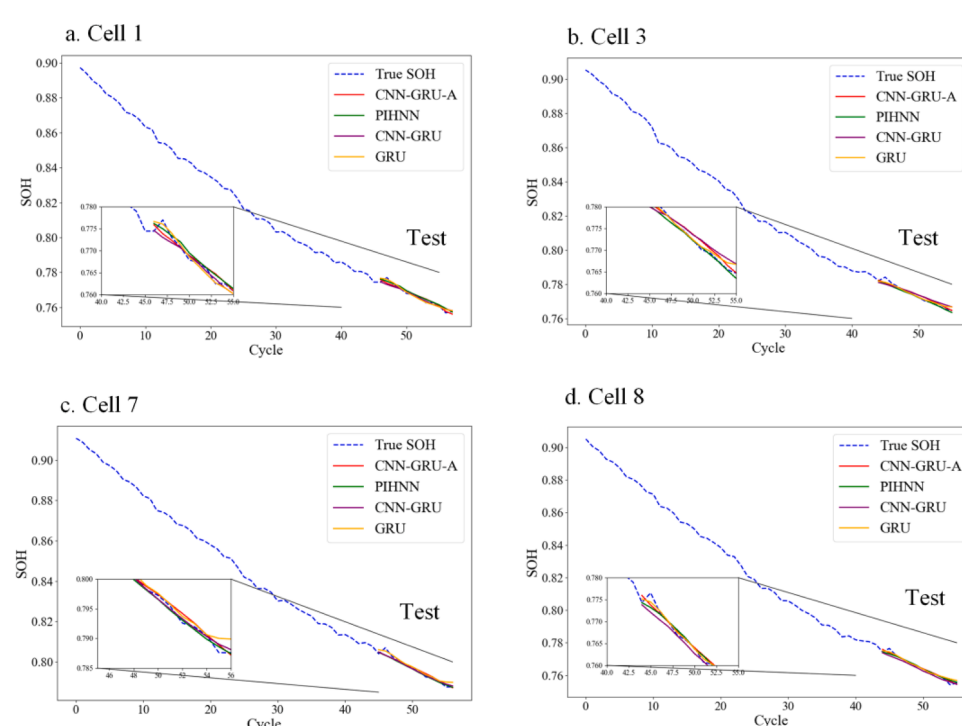


Fig. 9. Comparison of prediction performance for different models on the Oxford battery dataset.

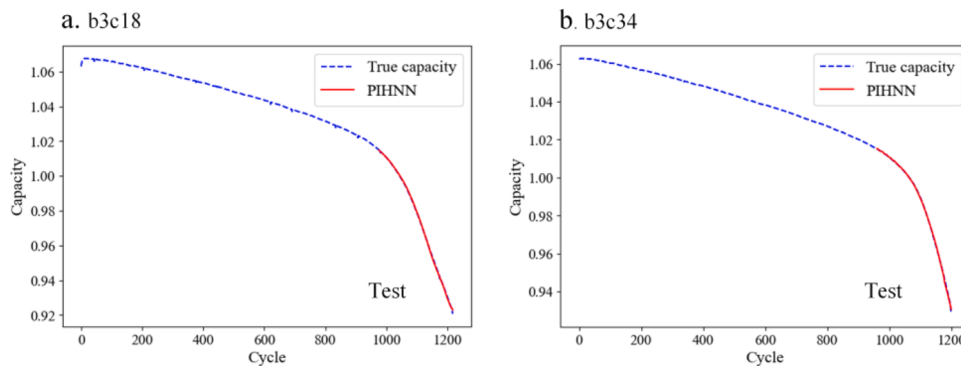


Fig. 10. The fitting curves of prediction.

Table 6

Comparison of prediction performance on the MIT battery dataset.

Cell	b3c18	b3c34
MAE (%)	PINHH	0.25
	PGTL-LSTM	0.31
RMSE (%)	PIHNN	0.33
	PGTL-LSTM	0.45

relationship between membrane resistance and capacity loss to enhance the model's physical consistency and predictive performance. Additionally, the introduction of the BOA significantly improved hyper-parameter configuration efficiency and reduced computational costs. Experimental results demonstrate that the PIHNN model outperforms traditional models in terms of MAE and RMSE under various operating conditions, showcasing exceptional prediction accuracy and robustness. This provides a novel solution for SOH estimation of LIBs.

In the future, as diversified data continues to accumulate and research into physical mechanisms advances, the PIHNN framework is expected to achieve greater adaptability and generality under dynamic and complex conditions. This will offer more reliable technical support for battery health management and safe operation.

Also note that both our private dataset in this work and the public dataset focus on full charge and full discharge scenarios. However, batteries do not necessarily complete the charging process entirely in real situations. In view of this, we would like to extend the present study to the situations of incomplete and irregular charging on the basis of the related studies (e.g., [27]).

CRediT authorship contribution statement

Yufu Luo: Writing – original draft, Visualization, Formal analysis, Conceptualization. **Shaokiao Ju:** Writing – original draft, Visualization, Formal analysis, Conceptualization. **Peichao Li:** Writing – review & editing, Supervision, Methodology, Funding acquisition. **Hengyun Zhang:** Methodology, Investigation, Data curation.

Declaration of competing interest

The authors declare that they have no known competing financial interests or personal relationships that could have appeared to influence the work reported in this paper.

Acknowledgments

This work was funded by the National Natural Science Foundation of China (grant nos 12272217 and 52476079).

Data availability

Data will be made available on request.

References

- [1] M. Yang, X. Sun, R. Liu, L. Wang, F. Zhao, X. Mei, Predict the lifetime of lithium-ion batteries using early cycles: a review, *Appl. Energy* 376 (2024) 124171, <https://doi.org/10.1016/j.apenergy.2024.124171>.
- [2] V.S.H.S. Che, J. Selvaraj, K.S. Tey, J.W. Lee, H. Shareef, R. Errouissi, State of health (soh) estimation methods for second life lithium-ion battery—review and challenges, *Appl. Energy* 369 (2024) 123542, <https://doi.org/10.1016/j.apenergy.2024.123542>.
- [3] X. Han, L. Lu, Y. Zheng, X. Feng, Z. Li, J. Li, M. Ouyang, A review on the key issues of the lithium ion battery degradation among the whole life cycle, *eTransportation* 1 (2019) 100005, <https://doi.org/10.1016/j.etran.2019.100005>.
- [4] S.W. Kim, K.-Y. Oh, S. Lee, Novel informed deep learning-based prognostics framework for on-board health monitoring of lithium-ion batteries, *Appl. Energy* 315 (2022) 119011, <https://doi.org/10.1016/j.apenergy.2022.119011>.
- [5] E. Braco, I. San Martín, P. Sanchis, A. Ursúa, D.-I. Stroe, State of health estimation of second-life lithium-ion batteries under real profile operation, *Appl. Energy* 326 (2022) 119992, <https://doi.org/10.1016/j.apenergy.2022.119992>.
- [6] Y. Zhang, Y.-F. Li, Prognostics and health management of lithium-ion battery using deep learning methods: a review, *Renew. Sustain. Energy Rev.* 161 (2022) 112282, <https://doi.org/10.1016/j.rser.2022.112282>.
- [7] X.-G. Yang, Y. Leng, G. Zhang, S. Ge, C.-Y. Wang, Modeling of lithium plating induced aging of lithium-ion batteries: transition from linear to nonlinear aging, *J. Power Source.* 360 (2017) 28–40, <https://doi.org/10.1016/j.jpowsour.2017.05.110>.
- [8] Y. Tang, M. Jia, L. Ai, B. Yin, Y. Cheng, Y. Liu, Capacity fade analysis of the lithium-ion power battery cycling process based on an electrochemical-thermal coupling model, *Energy Technol.* 3 (12) (2015) 1250–1259, <https://doi.org/10.1002/ente.201500196>.
- [9] S. Chen, Q. Zhang, F. Wang, D. Wang, Z. He, An electrochemical-thermal-aging effects coupled model for lithium-ion batteries performance simulation and state of health estimation, *Appl. Therm. Eng.* 239 (2024) 122128, <https://doi.org/10.1016/j.applthermaleng.2023.122128>.
- [10] P. Luo, P. Li, D. Ma, K. Wang, H. Zhang, A novel capacity fade model of lithium-ion cells considering the influence of stress, *J. Electrochem. Soc.* 168 (9) (2021) 090537, <https://doi.org/10.1149/1945-7111/ac24b5>.
- [11] X. Hu, F. Feng, K. Liu, L. Zhang, J. Xie, B. Liu, State estimation for advanced battery management: key challenges and future trends, *Renew. Sustain. Energy Rev.* 114 (2019) 109334, <https://doi.org/10.1016/j.rser.2019.109334>.
- [12] O. Demirci, S. Taskin, E. Schaltz, B.A. Demirci, Review of battery state estimation methods for electric vehicles-part ii: Soh estimation, *J. Energy Storage* 96 (2024) 112703, <https://doi.org/10.1016/j.est.2024.112703>.
- [13] X. Zhu, W. Wang, G. Zou, C. Zhou, H. Zou, State of health estimation of lithium-ion battery by removing model redundancy through aging mechanism, *J. Energy Storage* 52 (2022) 105018, <https://doi.org/10.1016/j.est.2022.105018>.
- [14] Z. Deng, L. Xu, H. Liu, X. Hu, Z. Duan, Y. Xu, Prognostics of battery capacity based on charging data and data-driven methods for on-road vehicles, *Appl. Energy* 339 (2023) 120954, <https://doi.org/10.1016/j.apenergy.2023.120954>.
- [15] Y. Huang, P. Zhang, J. Lu, R. Xiong, Z. Cai, A transferable long-term lithium-ion battery aging trajectory prediction model considering internal resistance and capacity regeneration phenomenon, *Appl. Energy* 360 (2024) 122825, <https://doi.org/10.1016/j.apenergy.2024.122825>.
- [16] K. Gao, Z. Huang, C. Lyu, C. Liu, Multi-scale prediction of remaining useful life of lithium-ion batteries based on variational mode decomposition and integrated machine learning, *J. Energy Storage* 99 (2024) 113372, <https://doi.org/10.1016/j.est.2024.113372>.
- [17] Y. Liu, G. Sun, X. Liu, Remaining useful life prediction of lithium-ion batteries based on peak interval features and deep learning, *J. Energy Storage* 73 (2023) 109308, <https://doi.org/10.1016/j.est.2023.109308>.

- [18] K. Zheng, J. Meng, Z. Yang, F. Zhou, K. Yang, Z. Song, Refined lithium-ion battery state of health estimation with charging segment adjustment, *Appl. Energy* 375 (2024) 124077, <https://doi.org/10.1016/j.apenergy.2024.124077>.
- [19] C. Li, L. Yang, Q. Li, Q. Zhang, Z. Zhou, Y. Meng, X. Zhao, L. Wang, S. Zhang, Y. Li, F. Lv, Soh estimation method for lithium-ion batteries based on an improved equivalent circuit model via electrochemical impedance spectroscopy, *J. Energy Storage* 86 (2024) 111167, <https://doi.org/10.1016/j.est.2024.111167>.
- [20] M. Raissi, P. Perdikaris, G.E. Karniadakis, Physics-informed neural networks: a deep learning framework for solving forward and inverse problems involving nonlinear partial differential equations, *J. Comput. Phys.* 378 (2019) 686–707, <https://doi.org/10.1016/j.jcp.2018.10.045>.
- [21] C. Xue, B. Jiang, J. Zhu, X. Wei, H. Dai, An enhanced single-particle model using a physics-informed neural network considering electrolyte dynamics for lithium-ion batteries, *Batteries* 9 (2023), <https://doi.org/10.3390/batteries9100511>.
- [22] J. Wang, Q. Peng, J. Meng, T. Liu, J. Peng, R. Teodorescu, A physics-informed neural network approach to parameter estimation of lithium-ion battery electrochemical model, *J. Power Source.* 621 (2024) 235271, <https://doi.org/10.1016/j.jpowsour.2024.235271>.
- [23] W. Li, J. Zhang, F. Ringbeck, D. Jöst, L. Zhang, Z. Wei, D.U. Sauer, Physics-informed neural networks for electrode-level state estimation in lithium-ion batteries, *J. Power Source.* 506 (2021) 230034, <https://doi.org/10.1016/j.jpowsour.2021.230034>.
- [24] H. Pang, L. Wu, J. Liu, X. Liu, K. Liu, Physics-informed neural network approach for heat generation rate estimation of lithium-ion battery under various driving conditions, *J. Energy Chem.* 78 (2023) 1–12, <https://doi.org/10.1016/j.jecchem.2022.11.036>.
- [25] F. Wang, Z. Zhai, Z. Zhao, Y. Di, X. Chen, Physics-informed neural network for lithium-ion battery degradation stable modeling and prognosis, *Nat. Commun.* 15 (1) (2024) 4332, <https://doi.org/10.1038/s41467-024-48779-z>.
- [26] C. Zhang, L. Tu, Z. Yang, B. Du, Z. Zhou, J. Wu, L. Chen, A cmmog-based lithium-battery soh estimation method using multi-task learning framework, *J. Energy Storage* 107 (2025) 114884, <https://doi.org/10.1016/j.est.2024.114884>.
- [27] C. Zhang, L. Luo, Z. Yang, B. Du, Z. Zhou, J. Wu, L. Chen, Flexible method for estimating the state of health of lithium-ion batteries using partial charging segments, *Energy* 295 (2024) 131009, <https://doi.org/10.1016/j.energy.2024.131009>.
- [28] X. Bao, L. Chen, A.M. Lopes, X. Li, S. Xie, P. Li, Y. Chen, Hybrid deep neural network with dimension attention for state-of-health estimation of lithium-ion batteries, *Energy* 278 (2023) 127734, <https://doi.org/10.1016/j.energy.2023.127734>.
- [29] L. Chen, S. Xie, A.M. Lopes, H. Li, X. Bao, C. Zhang, P. Li, A new soh estimation method for lithium-ion batteries based on model-data-fusion, *Energy* 286 (2024) 129597, <https://doi.org/10.1016/j.energy.2023.129597>.
- [30] S. Khaleghi Rahimian, M.M. Forouzan, S. Han, Y. Tang, A generalized physics-based calendar life model for li-ion cells, *Electrochim. Acta* 348 (2020) 136343, <https://doi.org/10.1016/j.electacta.2020.136343>.
- [31] K. Bischof, M. Flügel, M. Höglzle, M. Wohlfahrt-Mehrens, T. Waldmann, Aging mechanism for calendar aging of li-ion cells with si/graphite anodes, *J. Electrochim. Soc.* 171 (1) (2024) 010510, <https://doi.org/10.1149/1945-7111/ad1b7c>.
- [32] P. Luo, P. Li, D. Ma, K. Wang, H. Zhang, Coupled electrochemical-thermal-mechanical modeling and simulation of lithium-ion batteries, *J. Electrochim. Soc.* 169 (10) (2022) 100535, <https://doi.org/10.1149/1945-7111/ac9a04>.
- [33] P. Arora, R.E. White, M. Doyle, Capacity fade mechanisms and side reactions in lithium-ion batteries, *J. Electrochim. Soc.* 145 (10) (1998) 3647, <https://doi.org/10.1149/1.1838857>.
- [34] R. Fu, S.-Y. Choe, V. Agubra, J. Fergus, Development of a physics-based degradation model for lithium ion polymer batteries considering side reactions, *J. Power Source.* 278 (2015) 506–521, <https://doi.org/10.1016/j.jpowsour.2014.12.059>.
- [35] P. Yang, H.D. Yang, X.B. Meng, C.R. Song, T.L. He, J.Y. Cai, Y.Y. Xie, K.K. Xu, Joint evaluation and prediction of soh and rul for lithium batteries based on a gbls booster multi-task model, *J. Energy Storage* 75 (2024) 109741, <https://doi.org/10.1016/j.est.2023.109741>.
- [36] D. Ge, G. Jin, J. Wang, Z. Zhang, A novel data-driven iba-elm model for soh/soc estimation of lithium-ion batteries, *Energy* 305 (2024) 132395, <https://doi.org/10.1016/j.energy.2024.132395>.
- [37] Y.-Y. Soo, Y. Wang, H. Xiang, Z. Chen, Machine learning based battery pack health prediction using real-world data, *Energy* 308 (2024) 132856, <https://doi.org/10.1016/j.energy.2024.132856>.
- [38] Y. Yang, Y. Xu, Y. Nie, J. Li, S. Liu, L. Zhao, Q. Yu, C. Zhang, Deep transfer learning enables battery state of charge and state of health estimation, *Energy* 294 (2024) 130779, <https://doi.org/10.1016/j.energy.2024.130779>.
- [39] Z. Wang, H. Zhang, B. Li, X. Fan, Z. Ma, J. Zhou, An imfo-lstm_bigru combined network for long-term multiple battery states prediction for electric vehicles, *Energy* 309 (2024) 133069, <https://doi.org/10.1016/j.energy.2024.133069>.
- [40] K. Li, Y. Zhang, H. Liu, Y. You, L. Zeng, Y. Hong, Z. Zhang, Z. He, A novel temporal-frequency dual attention mechanism network for state of charge estimation of lithium-ion battery, *J. Power Source.* 622 (2024) 235374, <https://doi.org/10.1016/j.jpowsour.2024.235374>.
- [41] R.J. Jacques Molu, B. Tripathi, W.F. Mbasso, S.R. Dzonde Naoussi, M. Bajaj, P. Wira, V. Blazek, L. Prokop, S. Misak, Advancing short-term solar irradiance forecasting accuracy through a hybrid deep learning approach with bayesian optimization, *Result. Eng.* 23 (2024) 102461, <https://doi.org/10.1016/j.rineng.2024.102461>.
- [42] V. Selvaraj, I. Vairavasundaram, A bayesian optimized machine learning approach for accurate state of charge estimation of lithium ion batteries used for electric vehicle application, *J. Energy Storage* 86 (2024) 111321, <https://doi.org/10.1016/j.est.2024.111321>.
- [43] J. Keil, A. Jossen, Electrochemical modeling of linear and nonlinear aging of lithium-ion cells, *J. Electrochim. Soc.* 167 (11) (2020) 110535, <https://doi.org/10.1149/1945-7111/aba44f>.
- [44] C. Birk, Diagnosis and Prognosis of Degradation in Lithium-Ion Batteries, University of Oxford, 2017, <https://doi.org/10.5287/bodleian:KO2kdmYGg>.
- [45] C. Birk, Oxford Battery Degradation Dataset 1, University of Oxford, 2017, <https://doi.org/10.5287/bodleian:KO2kdmYGg>.
- [46] K.A. Severson, P.M. Attia, N. Jin, N. Perkins, B. Jiang, Z. Yang, M.H. Chen, M. Aykol, P.K. Herring, D. Fragedakis, M.Z. Bazant, S.J. Harris, W.C. Chueh, R. Braatz, Data-driven prediction of battery cycle life before capacity degradation, *Nat. Energy* 4 (5) (2019) 383–391, <https://doi.org/10.1038/s41560-019-0356-8>.
- [47] Q. Liu, Z. Shang, S. Lu, Y. Liu, Y. Liu, S. Yu, Physics-guided tl-lstm network for early-stage degradation trajectory prediction of lithium-ion batteries, *J. Energy Storage* 106 (2025) 114736, <https://doi.org/10.1016/j.est.2024.114736>.